Proceedings of the 1st Global Power and Propulsion Forum
GPPF 2017
Jan 16-18, 2017, Zurich, Switzerland
www.pps.global

GPPF-2017-128

APPLICATION OF SWEEP TO TRANSONIC COMPRESSOR ROTOR BLADES FOR LOW-ORDER STATISTICAL MOMENT AVERAGING IN ROBUST DESIGN

Jan Kamenik, Andy J. Keane, David J. J. Toal
Rolls-Royce University Technology Centre
University of Southampton
jkamenik@soton.ac.uk
Southampton, Hampshire, United Kingdom

Ron Bates
Rolls-Royce plc
ron.bates@rolls-royce.com
Derby, Derbyshire, United Kingdom

ABSTRACT

Robust design optimization involves finding the low-order statistical moments, i.e. the maximization of some mean quantity of interest and minimization of its variance. The question arises as to when a mean or variance value can be considered to be converged to an acceptable level of certainty. A designer naturally seeks to keep the number of function evaluations as low as possible when converging statistics. There is no general answer to the question of how many CFD simulations need to be carried out in order to obtain reliable estimators and which sampling methods perform better. Furthermore, multi-fidelity optimization techniques such as Co-Kriging can be used to combine different convergence levels and the question remains as to how many functions evaluations should be carried out. Practical guidelines applicable for the robust design optimization of turbomachinery blades are provided here. The applied methodology involves the freely available NASA Rotor 37 geometry and 3D steady-state RANS-based CFD with the Spalart-Allmaras turbulence model. The numerical CFD results are validated against actual experimental results. A uniformly distributed sweep uncertainty applied at the tip of the blade is propagated using Monte Carlo and Quasi-Monte Carlo-based sampling (low-discrepancy Halton and randomized Sobol sequence) for comparisons. Statistical post-processing of the results is based on 500 CFD runs for each sampling strategy. As an indicator of the error bounds, standard deviation and confidence intervals for the converging sample means of all quantities of interest are calculated. The required number of iterations is estimated.

INTRODUCTION

Modern aircraft engines and their individual components such as turbine and compressor blades are highly-optimized designs and subject to many uncertainties. Blade geometries in service now are the result of multi-objective optimization processes, involving a plethora of design variables, structural and performance constraints and many conflicting objectives. Such designs can be very sensitive to inevitable uncertainties, for example due to manufacturing tolerances, in-service deterioration or varying operating conditions. It has been shown in literature (e.g. [4, 14]) that such uncertainties, even very small perturbations on the order of tenths of millimetres, can lead to significant engine performance degradation. For compressor blades, aerodynamic performance considerations are of prime importance whereas for turbine blades the metal temperature is more crucial. Next generation computational modelling and scientific research therefore requires engineers and researchers to incorporate variations into the design process. This approach is termed robust design and typically involves the low-order statistical moments, that is maximization of some mean performance measure, such as the adiabatic efficiency, and simultaneous minimization of its variance. However, it is unclear how many simulations need to be carried out in order to obtain reliable estimators (i.e. converged to an acceptable margin of error), what errors can be considered acceptable and what sampling methods perform better than others by requiring fewer function evaluations for the same level of accuracy. Furthermore, different levels can be combined with multi-fidelity robust design optimization techniques such as Co-Kriging. How many simulations should be carried out for each level of fidelity? In the literature, Co-Kriging was for example used to optimize a 2D section of a Rolls-Royce compressor blade [6]. 100 LPτ samples were used to calculate more accurate, but computationally expensive converged sample means and 5 LPτ points were used to calculate less accurate but cheap estimates of the mean. Was this a good combination or is there a computationally cheaper, more efficient combination to get results with the same accuracy? Answers to these questions are sought in this paper.

METHODOLOGY

A commonly used 3D engineering parameter for turbomachinery blades, sweep is introduced as an uncertainty at the blade tip and 3D Reynolds-averaged Navier-Stokes

(RANS)-based steady-state computational fluid dynamics (CFD) using the Spalart-Allmaras turbulence model is used to evaluate the probabilistic outputs. Mean and variance of compressor performance quantities of interest such as adiabatic efficiency, pressure ratio and mass flow rate are calculated after every new CFD simulation to obtain convergence plots. Different sampling methods such as naive Monte Carlo (MC) and Quasi-Monte Carlo (QMC) methods based on low-discrepancy Halton and Sobol sequences are used. NASA Rotor 37 was chosen as a test case as it is freely available and experimental data for CFD validation exists. It is a low-aspect ratio transonic axial compressor rotor with 36 blades originally designed as an inlet stage for an eight-stage core compressor with a 20:1 pressure ratio. It rotates with 17188.7 rpm (1800 rad s^{-1}) and, as Dunham [3] remarks, is roughly representative of design and performance levels of transonic blades used in gas turbine compressors 15 years ago. One should note that NASA Rotor 37 is somewhat controversial as essentially all past numerical studies to some degree have inaccurately predicted adiabatic efficiency, pressure ratio as well as downstream profiles, prompting more and more research with an increasing level of fidelity (e.g. large eddy simulations (LES)) in order to account for this discrepancy between experimental and CFD results [7, 10]. There are discrepancies even with LES calculations, although they do perform slightly better than RANS-based simulations [5]. The case was employed here anyway as the geometry and boundary conditions are freely available and therefore allow for verifiable research results. What is more, the discrepancies themselves are of limited concern as emphasis is placed on the statistics of the quantities of interest, rather than as accurate as possible CFD. Nonetheless, of course all efforts are made to obtain as good as possible agreement with the experimental data using RANS-based CFD.

COMPUTATIONAL MODEL

The computational model of NASA Rotor 37 comprises the rotating rotor disk and stationary upstream and downstream disks on either side plus the stationary casing wall. The fillet at the hub is present but the small cavities between the hub and the rotor are closed and not modelled. Boundary conditions are given by Tartinville and Hirsch [13] and the rotor is running at peak efficiency. For this operating point, the static outlet pressure is set to 1.175 bar. The rotationally periodic CFD domain and model, defined via 21 radially stacked aerofoil sections, are shown in Fig. 1.

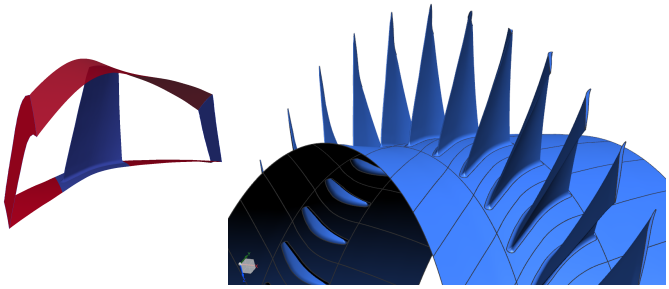

Fig 1: Computational model of NASA Rotor 37

The outlet is located 10.67 cm downstream of the blade hub leading edge and the inlet 4.19 cm upstream. The tip clearance at design speed is 0.356 mm. The blade hub fillet radius is 2.5 mm. The inlet turbulence intensity was estimated at 3%. Two cavities, 0.75 mm in width, 0.264 cm upstream and 4.521 cm downstream of the hub leading edge were present in the original experimental set-up but are not present in the model used here. All walls are adiabatic with no-slip boundary conditions. A subsonic inflow boundary condition is prescribed on the inlet and a subsonic outflow with radial equilibrium on the outlet. The fluid is air modelled as a perfect gas with constant specific gas constant 287.058 J kg^{-1} K^{-1} and ratio of specific heats of 1.4.

The computational workflow is based on Rolls-Royce's in-house RANS solver HYDRA. Meshing, the CFD setup and post-processing (using ParaView's Python API) is automated using Python and Matlab scripts. A flowchart of all steps involved in the workflow is shown in Fig. 2.

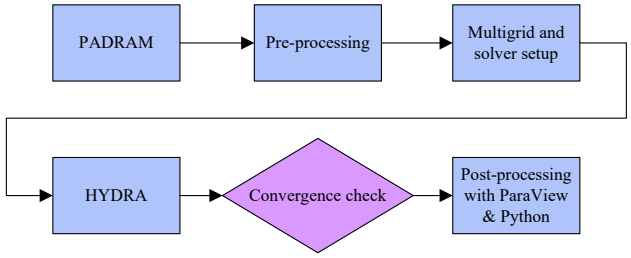

Fig 2: CFD workflow

A structured mesh was generated using Rolls-Royce's in-house mesher PADRAM with the default single passage mesh topology, namely up- and downstream H-meshes with an 0-mesh around the blade consisting of 12 layers and upper and lower H-meshes on the side. Mesh cells become denser near the blade LE and TE as well as near the hub and tip. In between, the cell density gradually decreases. A butterfly O-mesh with 15 layers is used in the tip gap. To permit the use of wall functions, a desired y^+ of above 30 was specified and the case was run to examine the actual y^+. y^+ values were found to lie in the desired region above 30 along the entire span height. Furthermore, a mesh independence study was carried out to determine the final mesh size. For the mesh independence study, the mean, mass-averaged absolute total outlet pressure was calculated using values from the last 100

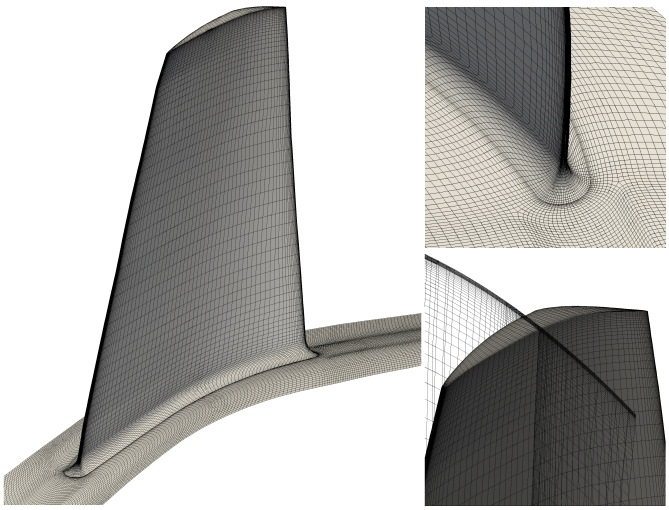

Fig 3: Mesh details

iterations. This mean was monitored whilst the mesh was continuously refined. The mesh was deemed to be grid independent once the percentage error change of these mean values was sufficiently small. The percentage error difference between the meshes with 1.37 and 2.06 million cells is only 0.036 %. This was deemed to be acceptable for the desired purpose and the mesh with 1.37 million cells was therefore selected as the final mesh, which is depicted in Fig. 3.

A steady-state RANS (Reynolds-averaged Navier-Stokes) approach using the one-equation Spalart-Allmaras turbulence model with wall functions is employed. A multigrid V-cycle scheme with 4 grid levels and 3 fine, 3 coarse and 3 pre- and post-smoothing iterations as well as first order smoothing after the second grid level was set up. 20 multigrid iterations were carried out on each grid. The change of the flow and turbulence residuals as well as the mass flow at the outlet were monitored to assess the convergence of the solution. All quantities were mass-averaged.

COMPRESSOR QUANTITIES OF INTEREST

The pressure increase of a compressor is measured by the total pressure ratio $\prod$ given by Eq. (1). Subscript 3 refers to the outlet, 2 to the inlet.

$$\Pi = \frac{p_{03}}{p_{02}} \tag{1}$$

$\prod$ is related to the total temperature ratio τ through the isentropic relation in Eq. (2):

$$\Pi = \left(\frac{T_{03}}{T_{02}}\right)^{\frac{\gamma}{\gamma-1}} = \tau^{\frac{\gamma}{\gamma-1}} \tag{2}$$

Another quantity of interest is the compressor isentropic efficiency η_{ad} defined in Eq. (3).

$$\eta_{ad} = \frac{\Pi^{\frac{\gamma-1}{\gamma}} - 1}{\tau - 1} \tag{3}$$

CFD VALIDATION

To validate the CFD results, experimental data and numerical results from references [6, 10, 11, 12] are used. It

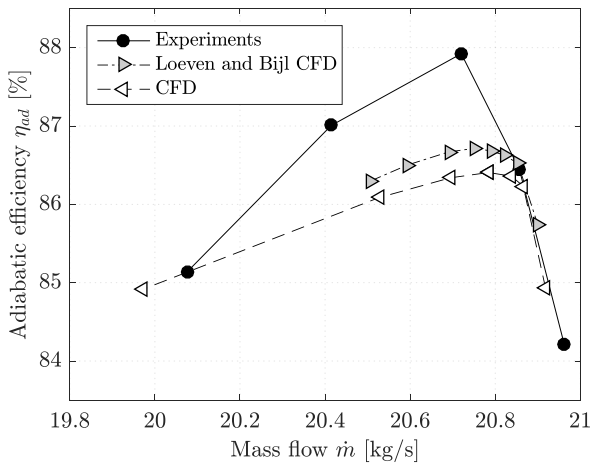

Fig 4: Compressor map validation - η_{ad}

Table 1: CFD validation with experimental data

Quantity	Experimental	Numerical	Error
$\dot{m}$ [kg/s]	20.74 ± 0.3	20.809	+0.33%
Π [−]	2.056	2.006	−2.43%
τ [−]	1.261	1.256	−0.40%
η_{ad} [%]	87.6	85.94	−1.89%

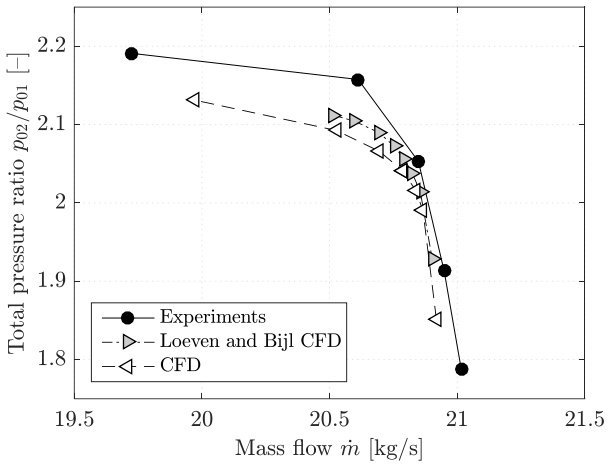

Fig 5: Compressor map validation - Π

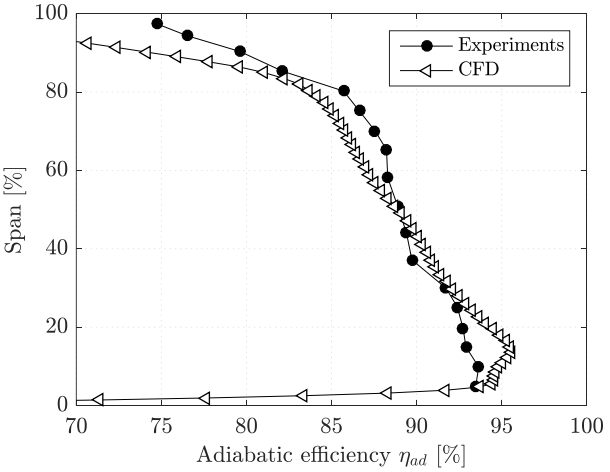

Fig 6: Pitchwise averaged outlet profiles - η_{ad}

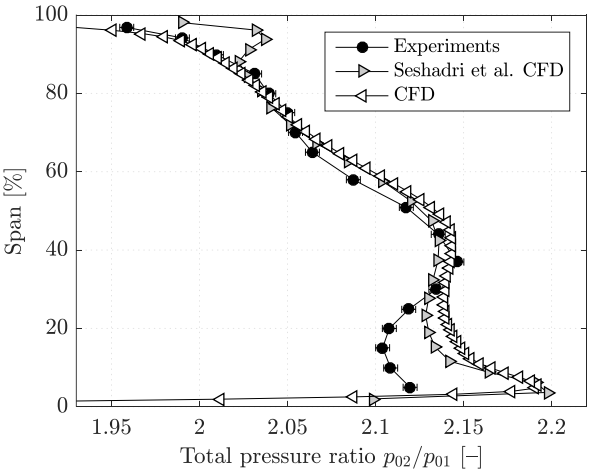

Fig 7: Pitchwise averaged outlet profiles - Π

should be noted that for the experimental data, measurement errors as given by Suder et al. [11] are ± 0.3 kg s^{-1} for massflow, ± 0.5 ° for flow angles, ± 0.01 N cm^{-2} for total pressures and ± 0.6 K for total temperatures. These errors are very small compared to the CFD discrepancies in some areas and can therefore be neglected. The percentage errors in Table 1 reveal that the maximum error of the CFD results is −2.43 % for the pressure ratio. With regard to the previously mentioned intricacies of Rotor 37, this is an acceptable error. Common for most CFD solvers, the adiabatic efficiency is underpredicted by 1.89%. The compressor map was computed and compared to the results from reference [10]. As depicted in Figs. 4-5, the results are close to the numerical results of reference [10], where the SST k-ω turbulence model was used instead. The CFD results do not match experimental results well in both cases however.

For further validation, pitchwise averaged profiles at the outlet are compared in Figs. 6-7. Overall, the results are very similar to the results from Seshadri et al. [10]. Similar to their results, the pressure ratio is overpredicted from 0 % to about 30 % span but accurate above 30 % span.

The most prominent feature of the flow is the shock wave, which emanates from the leading edge of the blade and impinges onto the suction side of the adjacent blade causing the flow there to separate. Loeven and Bijl [7] obtained about 1% more accurate quantities of interest with Spalart-Allmaras-based CFD and an additional transition model. Figure 8 depicts their results (on the left) and compares them with the results obtained in this study (on the right). It is evident that visually the differences, including the shock wave position, are very small and negligible. Again however, when comparing the CFD to experimental results (laser anemometer data), the CFD-predicted passage shock wave position on the mid-pitch line at 70% span is about 2.5 mm behind the measured experimental values [11].

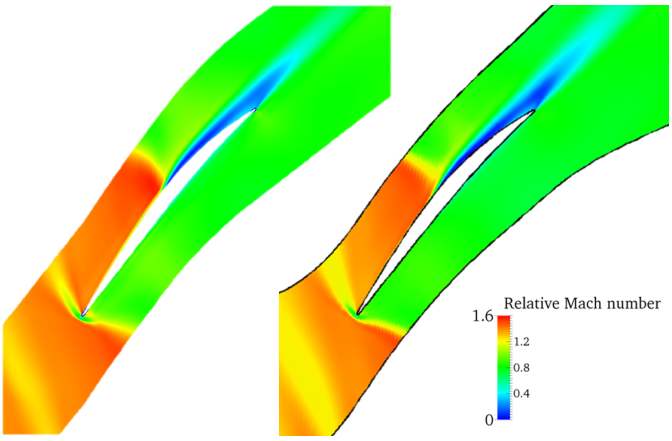

Fig 8: Shock wave position validation at 50% span

STATISTICAL MEASURES & SWEEP VARIATIONS

The Law of Large Numbers provides the statistical foundation of this investigation and guarantees consistent estimators: In the limit, as the sample size $n \to \infty$, the sample mean converges to the expected value, $x \to \mu$. The sample mean and the unbiased sample variance are defined according to Eqs. (4) and (5) [9]. In Eq. (6), the square of the variability of $\overline{x}$ depends inversely on the number of samples N and linearly on the relative fluctuation with itself, $\sigma / \overline{x}$, which is unknown. These statistics need to be estimated. Also, it is noteworthy that estimating the mean and other statistics is the same whether the underlying data comes from a model with just one uncertainty (as is the case here) or from a much more intricate model with many more parameters.

$$\overline{x} = \frac{1}{N}\sum_{i=1}^{N} x_i \tag{4}$$

$$\hat{s}^2_{N-1} = \frac{1}{N-1}\sum_{i=1}^{N} (x_i - \overline{x})^2 \tag{5}$$

$$\epsilon^2_{\overline{x}} = \frac{1}{N}\frac{\mathrm{Var}(x)^2}{\overline{x}^2} = \frac{1}{N}\left(\frac{\sigma}{\overline{x}}\right)^2 \tag{6}$$

Out of a range of 3D blade design parameters such as lean, sweep, skew, end wall profiling and LE or TE recambering, sweep was selected and applied at the blade tip. The application of forward or backward sweep at the blade tip is a common method of altering the tip flow to improve turbomachinery blade performance. Sweep is defined as the axial movement of blade sections along the engine axis and is known to affect the blade loading, shock strength, shock position and the stability margin, e.g. see Dixon and Hall [1] for details. This sweep uncertainty is distributed according to a uniform probability distribution function between ± 10 mm. Radially the deviation is modelled with a piece-wise cubic spline.

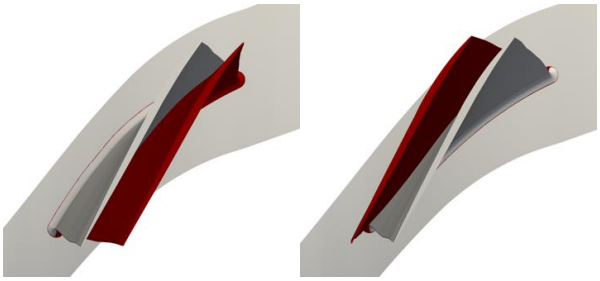

Fig. 9: Maximum sweep variations (red)

KNOWN KNOWNS & KNOWN UNKNOWNS

It is important to recognize that the effects from uncertainties to be modelled and propagated lead to higher variations in the quantities of interest than those from the computational approach itself. This leads to the common distinction of uncertainties in inherent (aleatoric) and model (epistemic) uncertainties. Model uncertainties could theoretically be fully removed if 100% accurate models existed. In contrast, inherent uncertainties such as manufacturing deviations cannot be removed from the model. Ultimately, it is important to ensure that model uncertainties from the mesh and residual oscillations are far smaller than the uncertainties one is intending to gauge the effects of. Here, effects from model uncertainties are two orders of magnitude smaller than effects from the introduced sweep uncertainty.

SAMPLING STRATEGIES

In general, the simplest way to propagate uncertainties is to use sampling strategies. A set of input points is selected at

which the model is evaluated deterministically and the statistics of interest are calculated using the results. The Monte Carlo (MC) method is the prime candidate. The MC method uses pseudo-random numbers based on an underlying probability distribution function. Convergence of the standard deviation of the error with $\mathcal{O}(1/\sqrt{N})$ is very slow. To improve the coverage and the efficiency, quasi-Monte Carlo (QMC) methods based on sets of points calculated deterministically using a discrepancy measure can be used. The main benefit of the use of low-discrepancy sequences is the improvement of the error convergence $\mathcal{O}((\log N)^d N^{-1})$. This comes at the drawback of introducing dependence on d-dimensions. Halton and Sobol sequences are used in this study. Whilst the Halton sequence is deterministic, the Sobol sequence was randomized (RQMC) using Matlab's Matousek-Affine-Owen algorithm (see Matoušek [8] for details). 500 individual CFD simulations were carried out using each sampling strategy.

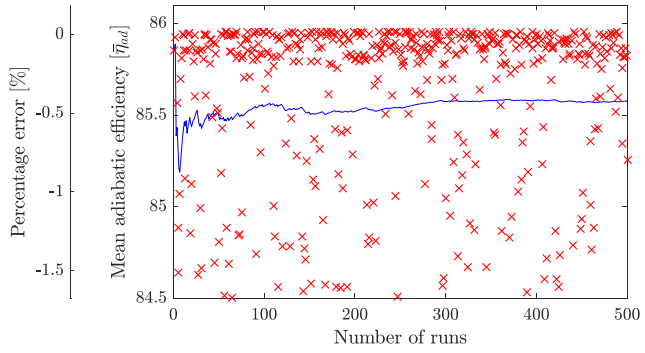

Fig 10: Observed values, percentage error & convergence of the adiabatic efficiency's sample mean using Monte Carlo results

CONFIDENCE INTERVALS OF THE MEAN

The main aim here is to estimate the required number of CFD runs to obtain robust estimates of mean output quantities and to compare the selected sampling methods' performances in doing so. In order to do this, the mean of each output was calculated. The law of large numbers then ensures that with an increasing number of CFD simulations, the sample mean converges to the expected value. The observed convergence of the sample mean and the data points are depicted in Fig. 10. On top of the mean, the standard deviation is required to estimate the dispersion. Since only 1 realization has actually been calculated, other paths are generated using curve fits of the output quantities of interest, which can quickly be evaluated thousands of times. Matlab's cubic smoothing splines implemented in the `csaps` function were used and 10000 paths were created for each sampling method. Figure 11 depicts the first 50 paths as an example. For the mean (i.e the mean of the mean), 95% confidence intervals can be calculated using Eq. (6) with significance level $\alpha = 0.05$ and $z_{0.025} = 1.96$

$$\overline{x} - z_{\alpha/2}\frac{\hat{s}}{\sqrt{N}} \leq \mu \leq \overline{x} + z_{\alpha/2}\frac{\hat{s}}{\sqrt{N}} \qquad (6)$$

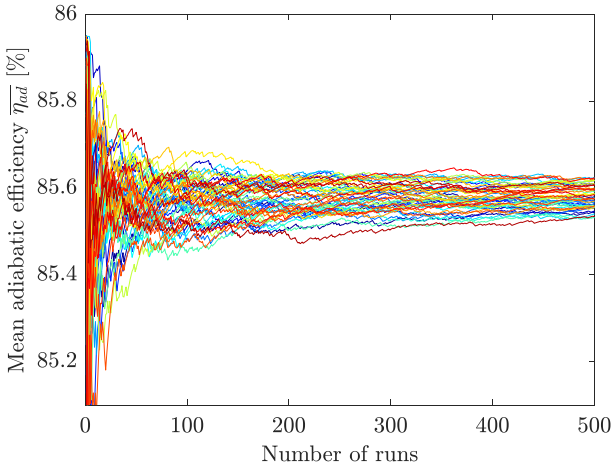

Figure 11: 50 simulated paths of the mean adiabatic efficiency with Monte Carlo

RESULTS AND DISCUSSION

By calculating Spearman's correlation coefficient for the sweep input and the output variables of interest, their dependence on sweep can be revealed. From this data, it is immediately apparent that the total pressure ratio and the total temperature ratio linearly depend on the sweep and their distributions are therefore close to the uniform input distribution. In contrast, adiabatic efficiency and mass flow

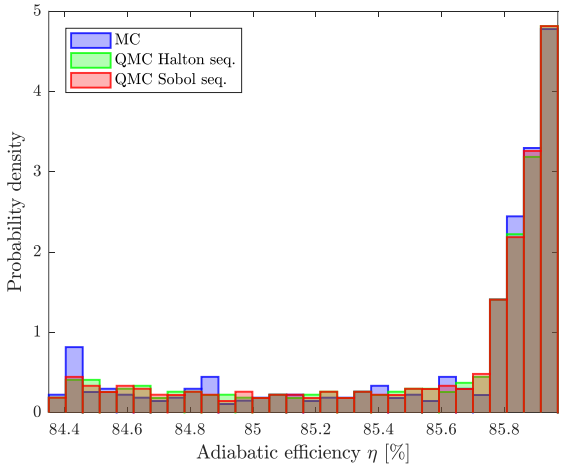

Fig 12: Histogram of the adiabatic efficiency

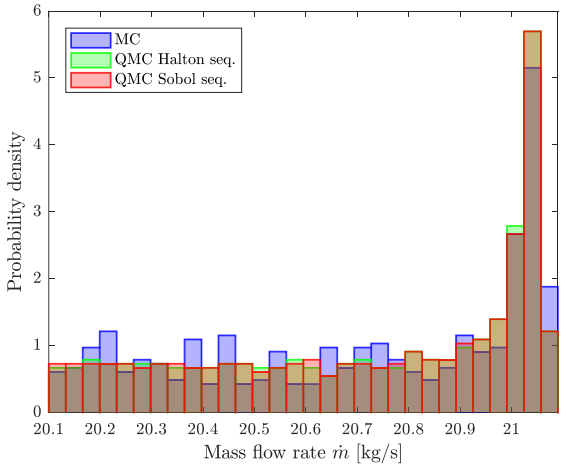

Fig 13: Histogram of the mass flow rate

depend nonlinearly on sweep and have skewed distributions. As an example, Figs. 12-13 show the resulting histograms for the adiabatic efficiency and the mass flow rate.

Figures 14-16 depict the 95% confidence intervals (CIs) of the averaged sample means for each output and for each method. It is evident that Quasi-Monte Carlo methods, regardless of the underlying sequence and scrambling, perform substantially faster than brute force Monte Carlo. As previously mentioned, this is of course to be expected. Halton and Sobol sequence-based sampling performance is virtually identical and the choice of the low-discrepancy sequence and whether or not it is scrambled does not matter. The majority of sweep variations worsen the adiabatic efficiency and consequently the expected value ends up about 0.4% below the deterministic value (where the rotor is running at peak efficiency). It is important to remember that these variations are based on a very high sweep range. Realistic deviations, for example from manufacturing variations, tolerances, tool wear, material property variations etc., are smaller. For realistic studies, experimental data can be used as the statistical basis.

Regardless, of prime interest are the confidence intervals depicted in Figs. 14-16. What is important then for a robust optimization workflow is to be able to calculate the sample means with some desired level of variance. Since for any sampling method, the computational effort required for acceptably converged results depends on the variance, no general statements or recommendations regarding the number of samples can be made. One would be wrong in assuming that the choice of just 5 LPτ points as the number of samples for each cheaply evaluated sample mean as in reference [6] would be sufficient in other cases as well. On the other hand, realistic deviations are smaller and evaluating only few number of points might be sufficient for a particular case. It is important to recognize that the shape of the 95% confidence intervals and hence the convergence rates in principle always remain the same for each method. Moreover, there will also always be some variance inherent to each sample mean regardless of the final number of iterations.

One possible way of estimating the required number of samples if the variance is known is by rearranging Eq. (6) and by introducing the error E, defined as $E = |\overline{x} - \mu|$, which leads to Eq. (7) [9]:

$$n = \left(\frac{z_{\alpha/2}\sigma}{E} \right)^2 \tag{7}$$

It is evident that Eq. (7) depends on the unknown population standard deviation σ, which can only be estimated from the data with the sample standard deviation $\hat{s}$, which is itself a random statistic. Therefore, the conclusion must be drawn that in order to calculate a required sample size with some confidence level, the only viable, general option is to use Eq. (7) to estimate this number. Essentially, this is the approach presented in reference [2]. In a multi-fidelity study, this method could for example be incorporated to calculate error bounds for the expensively estimated sample means and

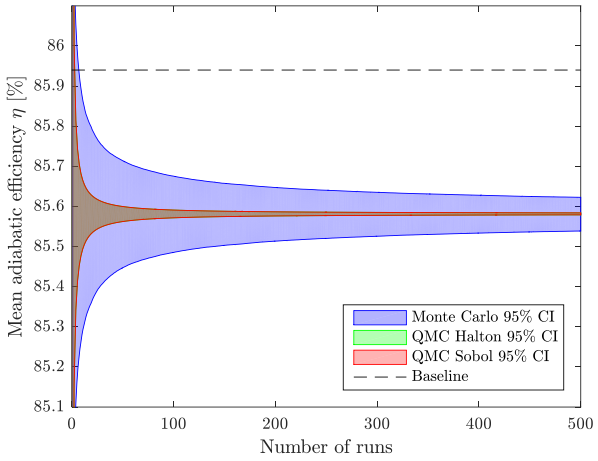

Fig 14: 95% confidence intervals of the mean adiabatic efficiency

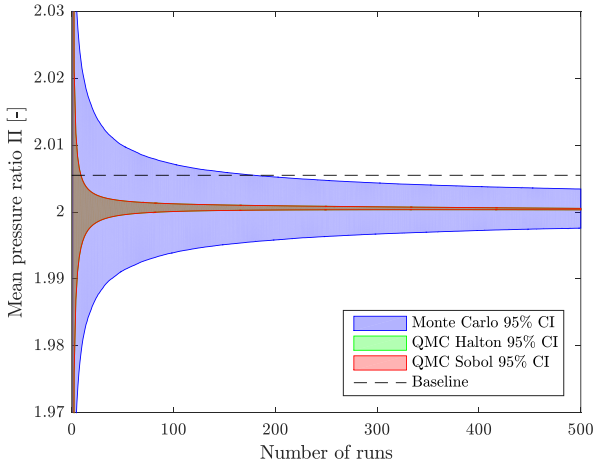

Fig 15: 95% confidence intervals of the mean pressure ratio

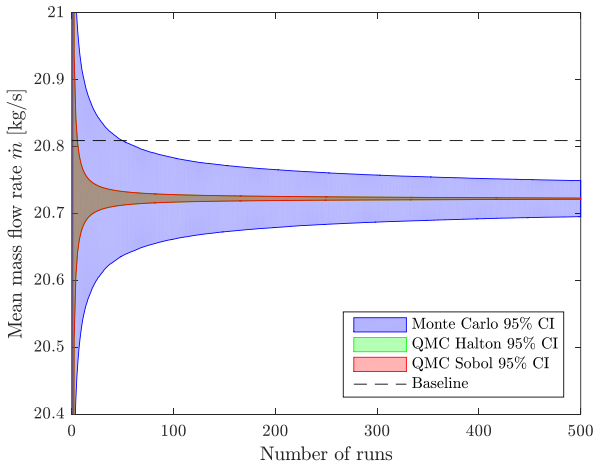

Fig 16: 95% confidence intervals of the mean mass flow rate

it can be displayed whilst the simulation is running. Equation (7) can also be written in terms of the percentage error [2]:

$$n = \left(\frac{100 z_{\alpha/2}\sigma}{PE\ \overline{x}} \right)^2 \tag{8}$$

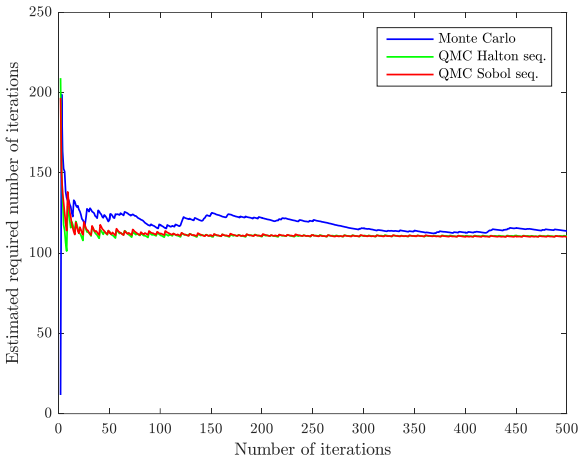

Fig 17: Estimated required number of iterations

As an example, the estimated number of iterations for the convergence of the sample mean for one of the output quantities, adiabatic efficiency, is shown in Fig. 17. From Fig. 10 it was evident that the percentage error ranges from about 0% to -1.5%. Specifying a desired percentage error of 0.01%, Fig. 17 reveals that in case of standard Monte Carlo the estimated number of required iterations for this desired accuracy is about 114. The interpretation is that at a level of 95% confidence the calculated adiabatic efficiency after this many iterations will be within 0.01% of the true population mean. As before and as expected, Quasi-Monte Carlo methods converge much quicker. Both suggest that the desired accuracy is reached after just 110 iterations. The difference of four iterations in the results (MC vs QMC) again highlights the stochastic nature of this procedure: In case of standard Monte Carlo, the estimated number of iterations is not yet converged. Note that Fig. 17 is based on the actually observed realizations of the sample mean and standard deviation of all 3 sampling methods. For Co-Kriging or other multi-fidelity techniques, the sample size for cheap function evaluations should be chosen in relation to the number of expensive CFD simulations and the confidence intervals in Figs. 14-16 can be used as an additional guideline.

CONCLUSIONS

In robust design optimization studies it is important to ensure the calculation of appropriately converged mean values. In the face of uncertainty, the challenges of the large computational requirements have to be met on one hand. On the other hand, convergence has to be ensured to within some degree of accuracy in order to obtain statistically significant or in other words trustworthy results. The procedure and the results presented here for the case of a compressor rotor can be implemented and used in similar robust design studies. In summary, the required number of iterations for a desired confidence level can be estimated and the method to do so can easily be implemented in robust design studies. Quasi-Monte Carlo methods outperform standard Monte Carlo and are preferable in terms of convergence.

ACKNOWLEDGEMENTS

Financial support from Rolls-Royce plc and the EPSRC Centre for Doctoral Training in Next Generation Computational Modelling grant EP/L015382/1 is acknowledged and greatly appreciated.

REFERENCES

[1] Dixon, S. L. and Hall, C., "*Fluid mechanics and thermodynamics of turbomachinery*", 7th ed., 2013, Butterworth-Heinemann.

[2] Driels, Morris R., and Young S. Shin. *"Determining the number of iterations for Monte Carlo simulations of weapon effectiveness"*, Naval Postgraduate School, 2004.

[3] Dunham, J., "*CFD validation for propulsion system components (la validation CFD des organes des propulseurs)",* Technical Report 355, 1998, DTIC Document.

[4] Goodhand, M. N., Miller, R. J., and Lung, H. W. "*The impact of geometric variation on compressor two-dimensional incidence range*". Journal of Turbomachinery, 2015, 137(2):021007.

[5] Hah, C. "*Large eddy simulation of transonic flow field in NASA rotor 37*". National Aeronautics and Space Administration, Glenn Research Center, 2009.

[6] Keane, Andy J. "*Cokriging for robust design optimization*." AIAA Journal 50.11: 2351-2364, 2012.

[7] Loeven, G. and Bijl, H., "*The application of the probabilistic collocation method to a transonic axial flow compressor",* 51st AIAA/ASME/ASCE/AHS/ASC Structures, Structural Dynamics and Materials Conference, 2010, American Institute of Aeronautics and Astronautics.

[8] Matoušek, J. "*On the L2-Discrepancy for Anchored Boxes",* Journal of Complexity, 1998, pp 14(4):527 - 556.

[9] Montgomery, Douglas C., and George C. Runger., *Applied statistics and probability for engineers*. John Wiley & Sons, 2010.

[10] Seshadri, P., Parks, G. T., and Shahpar, S., "*Leakage uncertainties in compressors: The case of rotor 37",* Journal of Propulsion and Power, 2014, pp 31(1):456 - 466.

[11] Suder, K. L., Chima, R. V., Strazisar, A. J., and Roberts, W. B., "*The effect of adding roughness and thickness to a transonic axial compressor rotor",* In ASME 1994 International Gas Turbine and Aeroengine Congress and Exposition, 1994, pp V001T01A113–V001T01A113, American Society of Mechanical Engineers.

[12] Suder, K. L., "*Experimental investigation of the flow field in a transonic, axial flow compressor with respect to the development of blockage and loss"*. PhD thesis, 1996, Case Western Reserve University.

[13] Tartinville, B. and Hirsch, C., Rotor 37. In Haase, Werner and Aupoix, Bertrand and Bunge, Ulf and Schwamborn, Dieter, editor, "*FLOMANIA - A European Initiative on Flow Physics Modelling: Results of the European-Union funded project, 2002 – 2004"*, 2006, chapter Rotor 37, pp 193–202, Springer Berlin Heidelberg.

[14] Wheeler, A. P., Sofia, A., and Miller, R. J. "*The effect of leading-edge geometry on wake interactions in compressors"*. Journal of Turbomachinery, 2009, 131(4):041013.